Linewidth Enhancement Factor in InAs/GaAs Quantum Dot Lasers and Its Implication in Isolator-Free and Narrow Linewidth Applications

Zeyu Zhang, *Student Member, IEEE*, Daehwan Jung, *Member, IEEE*, Justin C. Norman, *Member, IEEE*, Weng W. Chow, *Fellow, IEEE*, and John E. Bowers, *Fellow, IEEE*

***Abstract*—The linewidth enhancement factor (α_{H}) is an important parameter for semiconductor lasers. In this paper, we investigate, both theoretically and experimentally, the key parameters that affect α_{H} of InAs/GaAs quantum dot lasers. Both dot uniformity and doping density are found to be critical in achieving small α_{H} in quantum dot lasers. The prospects for quantum dot lasers in isolator-free and narrow linewidth applications are also discussed.**

***Index Terms*—Linewidth enhancement factor, quantum dot laser, feedback sensitivity, narrow linewidth.**

I. Introduction

ONE of the major differences of semiconductor lasers from their solid-state counterpart is the existence of a carrier reservoir in addition to the photon reservoir. As a result, the real and the imaginary part of the complex refractive index in the active region are coupled as an instantaneous change in carrier density in the laser active region changes both the material gain and real refractive index. This phenomenon manifests in semiconductor lasers as broadened spectral linewidth compared to what is predicted from the modified Schawlow-Townes linewidth formula [1]. Henry [2] was the first to properly explain the linewidth enhancement in semiconductor lasers with the introduction of the linewidth enhancement factor

$$\alpha_{\mathrm{H}} = -\frac{dn'/dN}{dn''/dN} \tag{1}$$

Manuscript received January 4, 2019; revised March 29, 2019; accepted May 7, 2019. Date of publication May 22, 2019; date of current version June 27, 2019. This work was supported in part by the Advanced Research Projects Agency-Energy under Grant DE-AR000067, by the U.S. Department of Energy under Contract DE-AC04-94AL85000, and by the American Institute for Manufacturing Integrated Photonics. *(Corresponding author: Zeyu Zhang.)*

Z. Zhang is with the Department of Electrical and Computer Engineering, University of California Santa Barbara, Santa Barbara, CA 93106 USA (e-mail: z_zhang@ucsb.edu).

D. Jung is with the Materials Department, University of California Santa Barbara, Santa Barbara, CA 93106 USA, and also with the Korea Institute of Science and Technology, Center for Opto-Electronic Materials and Devices, Seoul 02792, South Korea (e-mail: daehwan.jung.ucsb@gmail.com).

J. Norman is with the Materials Department, University of California Santa Barbara, Santa Barbara, CA 93106 USA (e-mail: jcnorman223@gmail.com).

W. Chow is with Sandia National Laboratories, Albuquerque, NM 87105 USA (e-mail: wwchow@sandia.gov).

J. E. Bowers is with the Department of Electrical and Computer Engineering and Materials Department, University of California Santa Barbara, Santa Barbara, CA 93106 USA (e-mail: bowers@ece.ucsb.edu).

Color versions of one or more of the figures in this paper are available online at http://ieeexplore.ieee.org.

Digital Object Identifier 10.1109/JSTQE.2019.2916884

where dn', dn'' are the variations in the real and imaginary part of the refractive index for a change in carrier density dN. An identical, yet independently developed, definition of the linewidth enhancement factor was shortly after reported by Vahala and Yariv [3] in their seminal paper on semiconductor noise theory. Both [2] and [3] derived the now well recognized linewidth formula for semiconductor laser:

$$\Delta\nu = \Delta\nu'_{\mathrm{ST}}(1+\alpha_{\mathrm{H}}^2) \tag{2}$$

where $\Delta\nu'_{\mathrm{ST}}$ is the modified Schawlow-Townes linewidth. The linewidth enhancement factor was soon found to be important in various aspects of semiconductor laser dynamics. In a laser feedback sensitivity study, the critical feedback level marking the onset of coherence collapse [4] was discovered to be strongly dependent on α_{H} [5], [6] from a stability analysis of the Lang-Kobayashi rate equation [7].

For quantum well (QW) lasers, α_{H} is normally in the range of 2-5 [8]–[10] depending on the active region composition and waveguide design. At these values, QW lasers experience significant linewidth broadening. The critical feedback level has been measured to be no larger than 10^{-4} times the output power [5]. The broadened linewidth has been proven to be detrimental to frequency-comb enabled high precision spectroscopy and optical atomic clock generation [11], [12]. The lack of feedback tolerance in QW lasers necessitates the introduction of an optical isolator into the package.

The reduction in active region dimensionality is an effective way to reduce α_{H} [13], [14]. In atom-like active regions as seen in quantum dot (QD) lasers, the carriers are confined in spatially separated potential boxes. For this reason, the variation in the index or gain in a dot is highly localized and will have little effect on another QD certain distance away. As pointed out by [15], the improved symmetry in the gain spectrum of QD laser also plays an important role in achieving smaller α_{H} compared to QW lasers. Due to the delta-like density of states, the ideal inhomogeneously broadened gain spectrum of a QD laser assumes a perfectly symmetrical gaussian shape. Granted the peak gain wavelength stays the same, the Kramer-Kronig relationship dictates a zero gain-peak differential refractive index and therefore zero α_{H} regardless of carrier density.

In real self-assembled QD lasers, several issues complicate the physics behind α_{H}. First, the band-filling effect and

many-body effects cause the gain peak wavelength to shift as carrier density increases [16]. Therefore, the actual α_{H} at the gain peak deviates from zero. Secondly, the Stranski-Krastanov growth of QDs creates dots with a size variation, which translates to an inhomogeneously broadened gain spectrum. Consequently, the α_{H} at any given wavelength is due to the contribution of an ensemble of dots, among which the on-resonance and off-resonance dots contribute differently. Furthermore, many of high performance QD lasers are modulation *p*-doped for improved device lifetime [17], temperature sensitivity [18] and modulation speed [19]. The introduction of *p*-type doping in the active region alters the position of the quasi-Fermi levels [20], which greatly affects α_{H} of QD lasers.

In this work, a many-body gain model is employed to calculate α_{H} in InAs/GaAs QD lasers. The importance of dot uniformity and modulation doping density in realizing small α_{H} will be demonstrated from both theoretical calculation and measurements. Considering the high feedback insensitivity of the QD lasers with small α_{H}, the possible application of these laser in future isolator-free system will be discussed. The effect of having small α_{H} in different narrow linewidth laser configurations will also be quantitatively studied.

II. Theoretical Model and Measurement Technique

Three batches of QD lasers with unintentionally doped (UID), 5×10^{17} cm^{-3}, and 1×10^{18} cm^{-3} *p*-type dopant concentration in the active region are grown and fabricated. These doping concentrations correspond to, on average, 0, 10, and 20 extra holes per QD. The lasers are otherwise the same as the ones reported before [21].

The theoretical modeling of QD active region starts from solving the equation of motion for the electron-hole polarization amplitude $p_{\alpha\beta}$:

$$\frac{dp_{\alpha\beta}}{dt} = i\omega_{\alpha\beta}p_{\alpha\beta} - i\Omega_{\alpha\beta}\left(n_{\alpha}^{e} + n_{\beta}^{h} - 1\right) + S_{\alpha\beta}^{c-p} + S_{\alpha\beta}^{c-c}, \tag{3}$$

where $\omega_{\alpha\beta}$ and $\Omega_{\alpha\beta}$ are the renormalized transition and Rabi frequencies, n_{α} and n_{β} are the electron and hole populations in states α and β. Dephasing contributions from carrier-phonon and carrier-carrier scattering are given by $S_{\alpha\beta}^{c-p}$ and $S_{\alpha\beta}^{c-c}$, respectively. The input to the calculations are the electron and hole energy levels, as well as the optical dipole matrix elements, computed using a Schrödinger-Poisson solver [22]. To connect the microscopic polarization amplitude $p_{\alpha\beta}$ with the macroscopic complex dielectric polarization amplitude $P(\omega)$, we utilize the relationship:

$$P(\omega) = \frac{1}{h}\sum_{\alpha}\sum_{\beta}\mu_{\alpha\beta}p_{\alpha\beta}, \tag{4}$$

where h is the Planck constant and $\mu_{\alpha\beta}$ is the dipole matrix element. The summation in (4) is over all QD and QW states. The material gain G_{M} and carrier induced phased change per distance $d\phi/dz$ is then directly proportional to $P(\omega)$ based on:

$$G_{\mathrm{M}}(\omega) = -\frac{\omega}{\varepsilon_0 ncVE(\omega)} Im\left(P(\omega)\right), \tag{5}$$

$$\frac{d\phi}{dz}(\omega) = -\frac{\omega}{\varepsilon_0 ncVE(\omega)} Re\left(P(\omega)\right), \tag{6}$$

where ε_0 and c are the permittivity and speed of light in vacuum, n is the background refractive index, $E(\omega)$ is the laser electric field amplitude, ω is its frequency, V is the dot-in-a-well (DWELL) volume. Details for the formulation and evaluation of eqs. (3) to (6) are described in the literature [16].

The calculation in (5) and (6) are for a homogeneous population of QD. For the presence of inhomogeneous broadening due to QD size fluctuations, we performed a statistical average over a range of band-gap energy ε:

$$S_{\mathrm{inh}}(\omega) = \int_{-\infty}^{\infty} d\varepsilon \frac{1}{\sqrt{2\pi}\Delta_{\mathrm{inh}}} \exp\left[-\left(\frac{\varepsilon - \varepsilon_g}{\sqrt{2}\Delta_{\mathrm{inh}}}\right)^2\right] S(\omega, \varepsilon), \tag{7}$$

where S refers to either G_{M} or $d\phi/dz$, ε_g is the InAs band-gap energy, and we assume a weighting described by a normal distribution characterized by an inhomogeneous broadening width Δ_{inh}. Following the formal definition of the linewidth enhancement factor, the α_{H} is then calculated from:

$$\alpha_{\mathrm{H}} = -\frac{\frac{d(d\phi/dz)_{\mathrm{inh}}}{dN}}{\frac{d(G_{\mathrm{M}})_{\mathrm{inh}}}{dN}}. \tag{8}$$

The experimental characterization of α_{H} involves directly measuring the change of real and imaginary parts of the complex refractive index. After Fabry-Perot (FP) laser sample preparation, amplified spontaneous emission (ASE) spectra are measured at different current injection levels under pulsed conditions. The mode-sum method [23] is then employed to extract the change of gain (Δg) and thereby the change of the imaginary part of the index (n'') from the ASE spectra. The change of the real part of the index (n') can be extracted by tracking the wavelength shift of the peaks of the FP modes ($\Delta\lambda_{\mathrm{m}}$). α_{H} can then be extracted based on

$$\alpha_{\mathrm{H}} = -\frac{dn'/dN}{dn''/dN} = -\frac{\frac{n'}{\lambda}\Delta\lambda_{\mathrm{m}}}{\frac{\lambda}{4\pi}\Delta g} = -\frac{4\pi n'}{\lambda^2}\frac{\Delta\lambda_{\mathrm{m}}}{\Delta g}. \tag{9}$$

III. Results and Discussion

The simulated homogeneously broadened spectra of G_{M} and $d\phi/dz$ are shown in Fig. 1(a)(b), respectively. The nonzero gain bandwidth in (a) is due to the many-body collisions represented by $S_{\alpha\beta}^{c-p}$ and $S_{\alpha\beta}^{c-c}$ in (3). These collisions result in a finite life time of carriers at certain energy state. Through quantum mechanics, the finite life time is translated to full-width-at-half-maximum (FWHM) of $\sim$5 meV in the homogeneously broadened gain spectrum of the QD laser. The red-shifted emission energy is due to bandgap renormalization from Coulomb coupling between discrete QD states and continuum states in the QW [24], [25].

Due to the small gain bandwidth in the homogeneous QD population, the carrier induced phase change shows strong wavelength dependence (Fig. 1(b)). At photon energy more than 10 meV away from gain peak, the refractive index decreases with increasing carrier injection. Such dependence on the carrier density gives rise to positive α_{H} and is commonly observed

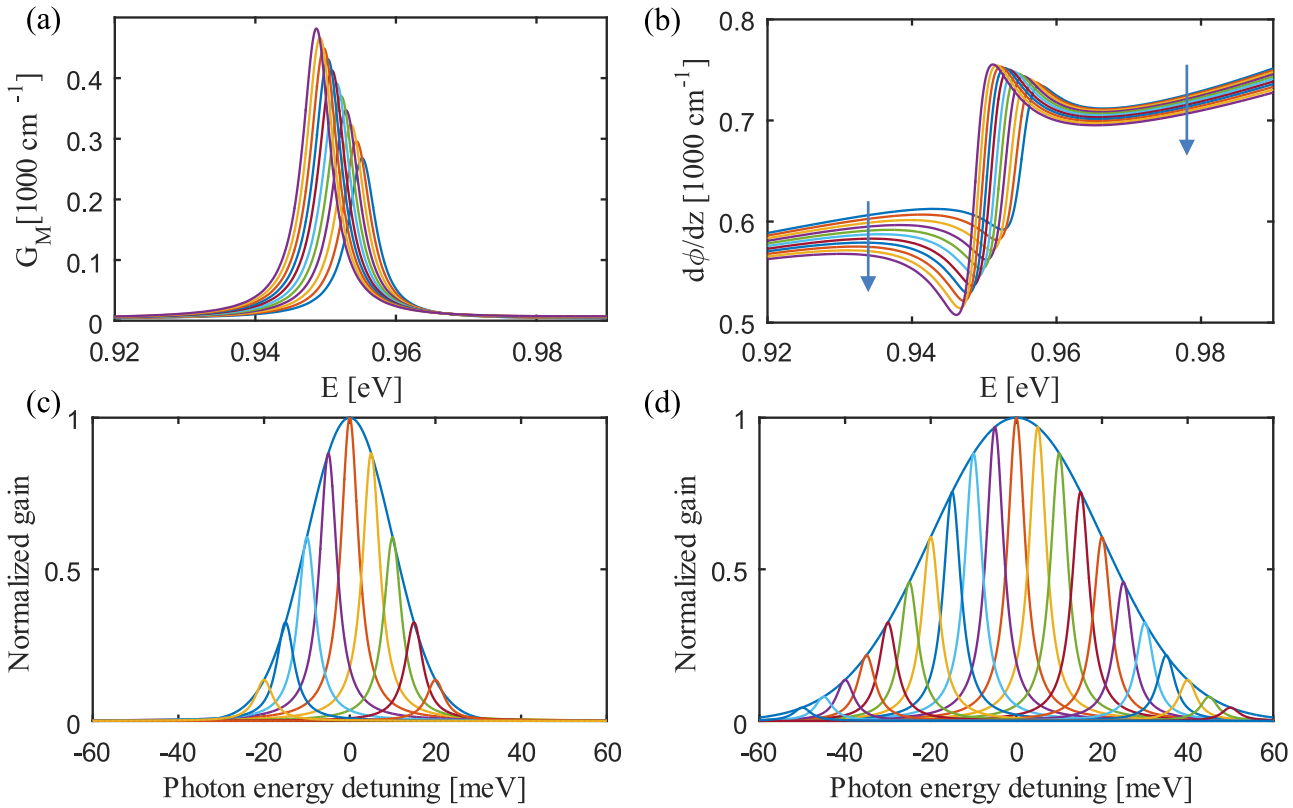

Fig. 1. (a)(b) Simulated homogeneously broadened spectra of G_{M} and $d\phi/dz$ at ground state in an undoped QD laser active region at carrier density from 2×10^{11} cm^{-2} to 3×10^{11} cm^{-2}. The area dot density is 1×10^{10} cm^{-2}. The arrows in (b) points to the direction of increasing carrier density. (c)(d) Schematic representations of how the inhomogeneous broadened gain spectrum of a QD laser is composed of contribution of dot groups with different emission energy. In (c), $\Delta_{\mathrm{inh}} = 10$ meV. In (d), $\Delta_{\mathrm{inh}} = 20$ meV.

in QW lasers [26]. In addition, since the differential gain at the tail of the gain spectra is very small, the absolute value of α_{H} at said wavelength regime becomes fairly large. At the gain peak wavelength, however, the refractive index increases with increasing carrier injection. This is due to bandgap renormalization that red shifts the peak emission wavelength. Therefore, the model predicts a negative α_{H} at wavelengths around gain peak in homogeneous QD population.

Since the inhomogeneously broadened gain spectrum is the weighted sum of homogeneoussly broadened spectra of QD with different sizes, in a realistic QD active region α_{H} at any wavelength is also the weighted sum of its homogeneous counterparts. Fig. 1(c)(d) provide insightful illustration on how dot size variation (Δ_{inh}) affects α_{H} at gain peak in QD lasers. In both Fig. 1(c)(d), the peak gain of QD active region mainly comes from the contribution of a homogeneous QD group with highest dot density. Due to the small homogeneous gain bandwidth, QD groups more than 10 meV detuned from the laser gain peak barely contributes to the peak gain, in spite of their significant population. However, the same detuned QD groups, as pointed out before, also show large positive α_{H} at the peak of the inhomogeneously broadened laser gain spectrum (the tail of their own homogeneously broadened spectra). Comparing Fig. 1(c) and (d), it can be seen that the larger Δ_{inh} is, the more the contribution from these detuned QD group to α_{H} at gain peak. As dot uniformity in the QD active region improves, the QD groups within the 10 meV detuning range will dominate the behavior of α_{H} of the laser. The QD active region satisfying this condition is expected to show close to zero or even negative α_{H}. The calculated α_{H} of an undoped QD active region at different Δ_{inh} is shown in Fig. 2. The effects of detuned dot groups on the gain-peak α_{H} can be clearly seen in Fig. 2(a). A homogeneous dot group originally shows negative alpha at the gain peak. As the dot size variation worsens, α_{H} at the gain peak increases due to large α_{H} at tails of the detuned dot groups. For Δ_{inh} larger than 10 meV, the gain-peak α_{H} begins to be dominated by the behavior of the detuned dot groups. The dependence of gain-peak α_{H} on carrier density at different Δ_{inh} is shown in Fig. 2(b). It can be seen that dot size variation not only modifies the gain-peak α_{H}, it also alters the trends of α_{H} versus carrier density. By comparing the gain bandwidth of the calculated inhomomogeous broadened gain spectrum with that of the measured gain spectrum extracted from ASE spectrum, the Δ_{inh} in our lasers is determined to be $\sim$10 meV [21]. The high dot uniformity in these lasers enables the gain-peak Δ_{inh} to be less affected by the detuned dot group.

When *p*-type doping is introduced in the QD active region, the quasi-Fermi levels in the conduction and valence band will be shifted down to lower energy. The movement of the quasi-Fermi levels causes a reduced transparent carrier density and increased differential gain in the laser active region [20], [27]. The effects of *p*-type dopants on the material gain and

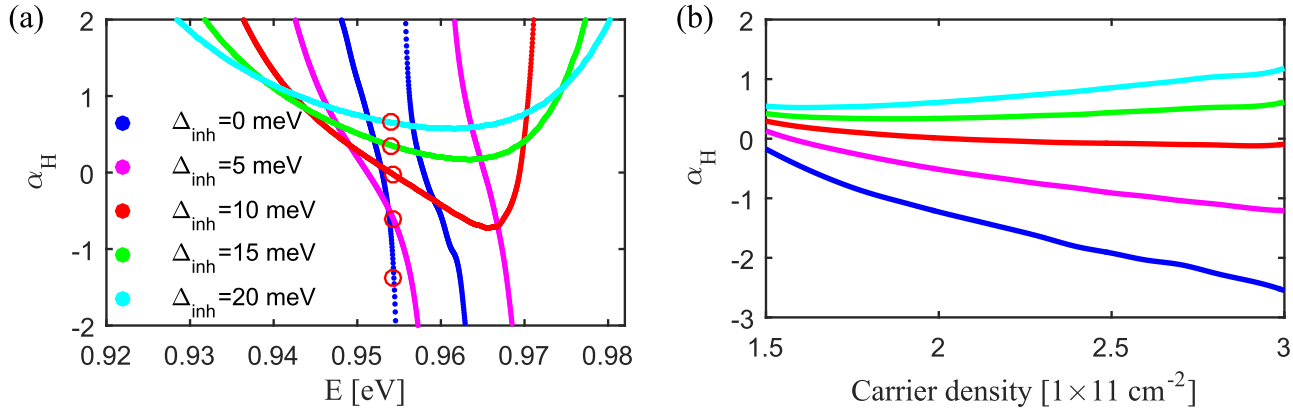

Fig. 2. (a) Calculated spectra of α_{H} at the ground state of an undoped QD active region under different inhomogeneous broadening at carrier density of 1×10^{11} cm^{-2}. The red circles mark α_{H} at the gain peak wavelength under each inhomogeneous broadening condition. (b) Calculated gain-peak α_{H} as a function of carrier density and inhomogeneous broadening. The traces from bottom up are for $\Delta_{\mathrm{inh}} = 0, 5, 10, 15$ and 20 meV.

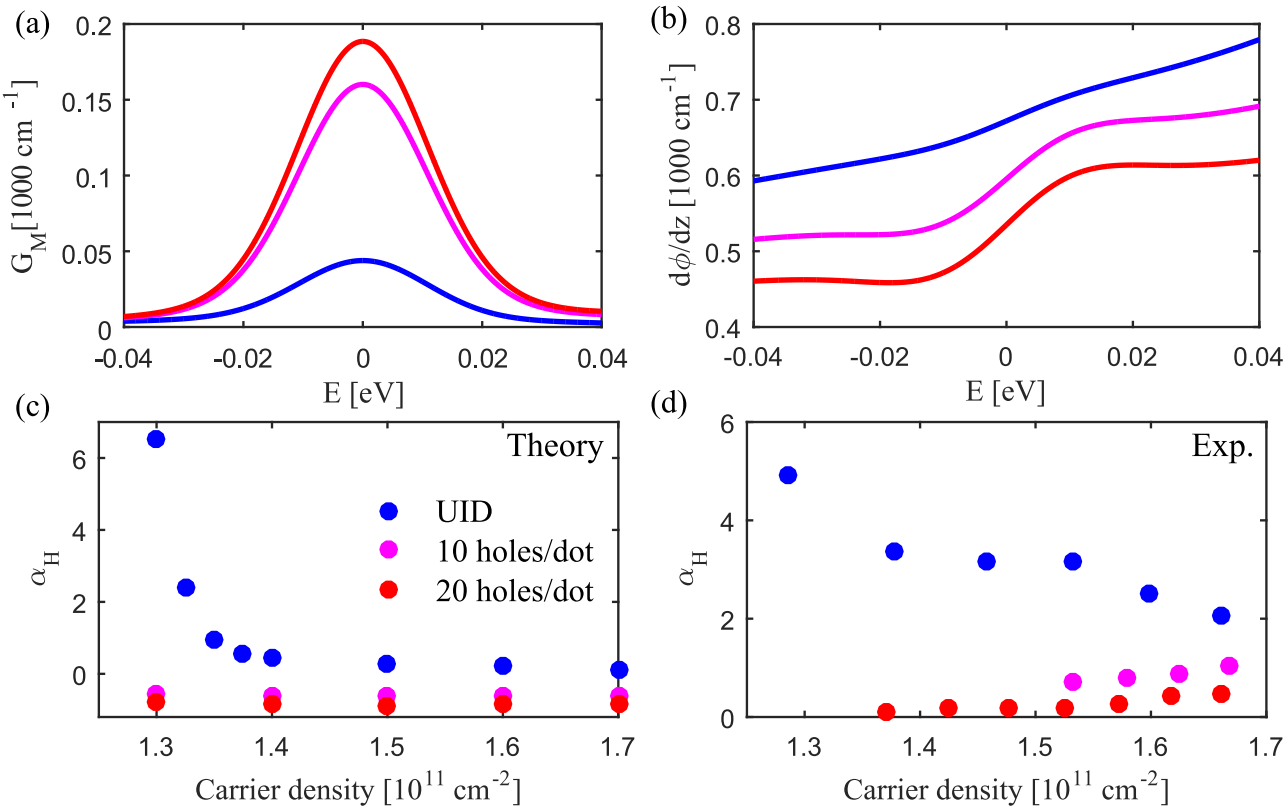

Fig. 3. (a)(b) Simulated inhomogeneously broadened spectra of G_{M} and $d\phi/dz$ at the ground state in QD laser active regions with different p doping levels. The blue, pink and red lines in (a) and (b) represent doping density of on average 0, 10 and 20 extra holes per dot. The calculation in both (a) and (b) are done at a carrier density of 1.7×10^{11} cm^{-2} and Δ_{inh} of 10 meV. (c)(d) Calculated and measured gain-peak α_{H} of the QD active region with Δ_{inh} of 10 meV. UID: unintentionally doped.

refractive index of the QD active region are shown in Fig. 3(a)(b). Due to lower transparency and higher differential gain, the p doped QD active region shows significantly higher material gain (Fig. 3(a)). The additional holes from the dopants also further decreases the refractive index compared to the undoped case(Fig. 3(b)). The calculated and measured gain-peak α_{H} are shown in Fig. 3(c)(d). For the UID laser, the sharp increase in α_{H} close to 1.3×10^{11} cm^{-2} results from the QD active region going through transparency at said carrier density. Due to the aforementioned changes in G_{M} and $d\phi/dz$ with doping density, both the calculation and measurement indicates decreased gain-peak α_{H} with increasing doping density. Despite the similar dependence on carrier density and doping density, the measured α_{H} is larger compared to the calculated counterpart. This is probably due to the fact that the model only calculates α_{H} in a single layer of DWELL, while the measured α_{H} is from the

extracted changes in gain and refractive index experienced by the entire optical mode. For this reason, any build up of carrier in regions other than the DWELL active region could cause the model to underestimate α_{H}. Nevertheless, the measured α_{H} in doped samples is still significantly smaller than what has been observed in QW lasers. More importantly, *p* doping in QD lasers provides a way to engineer the α_{H} with the additional benefits of improved modulation speed [19] and device reliability [17]. Through further improvement in dot uniformity, reduction of laser threshold through high reflective (HR) coating, or having more doping density in the QD active region, closer to zero [28] or even negative α_{H} could be achieved.

IV. Isolator-Free Operation With Quantum Dot Lasers

Now that the ingredients for obtaining small α_{H} in QD semiconductor lasers are well understood, it is necessary to consider the practical implementations of these lasers in applications where small α_{H} is crucial to proper performance. The first type of applications to be considered here are diode laser packages requiring low optical feedback sensitivity. In almost all commercial butterfly packaged tunable lasers or narrow linewidth lasers, co-packaged optical isolators can be found to ensure larger than 30 dB optical isolation [29], [30]. These isolators must be installed because the QW lasers in these package typically only tolerate feedback level up to 10^{-4} times the output power [5]. The inclusion of optical isolators in the laser assembly increases the packaging complexity and the overall cost of the product. It is therefore highly desired to eliminate the co-package optical isolator yet still maintain the feedback tolerance of the product.

In semiconductor stability analysis, when the ratio of laser power reflected back into the laser cavity reaches above a certain threshold, the laser will operate in the regime of coherence collapse marked by severely broadened laser linewidth and rapidly deteriorated laser relative intensity noise (RIN) [4]. The threshold for the feedback power ratio is called critical feedback level (f_{crit}). From a small signal analysis of the Lang-Kobayashi rate equation [7], f_{crit} manifests as the feedback level where the system just starts to acquire an unstable pole. f_{crit} turns out to be a strong function of α_{H} especially when α_{H} is smaller than 1, as in the case of a QD laser. The relationship between f_{crit} and α_{H} can be described by [5], [31]:

$$f_{\mathrm{crit}} = \frac{\tau_{\mathrm{L}}^2 (K f_{\mathrm{r}}^2 + \gamma_0)^2}{16C^2} \frac{1+\alpha_{\mathrm{H}}^2}{\alpha_{\mathrm{H}}^4}, \tag{10}$$

where τ_{L} is the round-trip time in the laser cavity, f_{r} is the relaxation oscillation rate, and $C = (1-R)/2\sqrt{R}$ is the coupling strength from the laser main cavity to the external cavity from a laser facet with reflectivity R. The term $K f_{\mathrm{r}}^2 + \gamma_0$ is known as the damping factor γ, in which K is the proportionality factor between γ and f_{r}^2 and γ_0 is the damping factor offset. Alternative forms of the critical feedback level have been proposed in the literature [32], [33]. However, they are limited in the range of applicable feedback intensity and α_{H}. (10) is chosen here since it best approximates the exact numerical solution from the Lang-Kobayashi equation, and for this reason is applicable to practically all feedback intensity and α_{H} [5], [6].

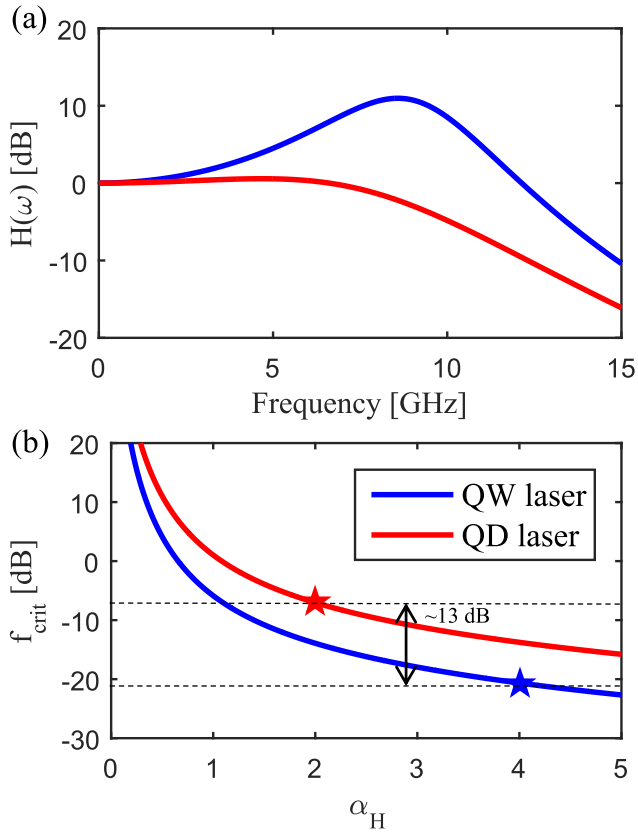

Fig. 4. (a) Calculated modulation response of a QW laser and a *p*-doped QD laser in this work. Both lasers are in-plane Fabry-Perot lasers. The transport effects and the interaction between the ground state and excited state of the QD active region are not considered in the calculation. More involved dynamic analysis can be found in [34]. (b) Estimated critical feedback level of the QW and QD lasers under discussion. The stars marks the possible operation points of the lasers above threshold. 0 dB represents 100% reflection. (10) is an approximated solution in the regime of small α_{H}. The exact solution gives even higher f_{crit} for $\alpha_{\mathrm{H}} < 1$ [6].

In (10), the quantities related to the intrinsic properties of the laser active region are γ and α_{H}. Therefore, both damping of the relaxation oscillations and α_{H} affect the f_{crit} of semiconductor lasers. The laser modulation response along with the relationship between f_{crit} and α_{H} are plotted in Fig. 4(a)(b) for a QW and a QD laser. The QD laser parameters used in the calculation in Fig. 4 are extracted from experiment. The key parameters and extraction procedure are discussed in Appendix A. The QW laser considered here assumes the same cavity design and relaxation oscillation frequency as the QD laser but different K-factor. In a diode laser, f_{r}^2 and γ are linearly related by the proportionality factor K, which depends on how the laser gain is compressed by the photon density in the cavity. In a QD lasers, the gain compression factor is reported to be at least 10 times that in a typical QW laser [35]. Consequently, the lowest K-factor reported in QD lasers is in the range of 0.7–0.9 ns [36], [37], while the lowest K-factor in QW lasers is in the range of 0.2–0.3 ns [38], [39]. The significant damping in QD lasers causes most modulation experiments to show a

lack of pronounced relaxation oscillation peaks as shown in Fig. 4(a). When feedback is presented in the system, the laser relaxation oscillation response will be superimposed with strong parasitic oscillation that distablizes the laser [6]. The roughly 3 times higher K-factor in QD lasers reduces the impact of such parasitic oscillation and makes QD lasers to be ~10 dB better than QW lasers based on (10), granted that all other parameters are the same. In addition, the much smaller α_{H} in QD lasers further enhances the tolerance to feedback. The smallest α_{H} at threshold observed in our experiment is ~0.5 as shown in Fig. 3(d). Considering the nonpinned carrier density above threshold in QD laser [40], α_{H} increases significantly above threshold [28]. Assuming four-fold increase in α_{H} above threshold, the QD laser is still predicted to tolerate up to 20% of optical feedback (Fig. 4(b)). Such behavior has been recently observed in feedback sensitivity experiments [41]. Feedback tolerance at this level is more than sufficient to warrant the future application of QD lasers in isolator-free laser packages.

V. Quantum Dot Lasers in Narrow-Linewidth Applications

The discovery and naming of α_{H} is closely tied to the optical linewidth of semiconductor lasers [1]. Knowing the ultra-low α_{H} in QD lasers, perhaps the most obvious applications of these laser are in systems with stringent linewidth requirement. In the receiver of a coherent communication system, for example, narrow linewidth lasers as low noise local oscillators are crucial in restoring the information encoded in the phase quadrature. Narrow linewidth operation of semiconductor lasers has been achieved through coupling with high-Q resonators in external cavity [42] or lateral confinement engineering in heterogeneous laser cross-section [43]. In the latter case, the dependence of laser linewidth on α_{H} follows (2). In the former case, due to the presence of the external cavity, the laser linewidth formula is modified as:

$$\Delta\nu = \Delta\nu'_{\mathrm{ST}} \frac{1+\alpha_{\mathrm{H}}^2}{F^2}, \tag{11}$$

where F is the linewidth reduction factor due to the external cavity. It is defined as:

$$F = 1 + A + B \tag{12}$$

$$A = \frac{1}{\tau_{\mathrm{L}}} \frac{d\phi_{\mathrm{ext}}}{d\omega} = \frac{\tau_{\mathrm{ext}}}{\tau_{\mathrm{L}}} \tag{13}$$

$$B = \frac{\alpha_{\mathrm{H}}}{\tau_{\mathrm{L}}} \frac{1}{r_{\mathrm{ext}}} \frac{dr_{\mathrm{ext}}}{d\omega}. \tag{14}$$

In (13) and (14), ϕ_{ext} and r_{ext} are the phase and magnitude of the effective mirror response of the external cavity. (13) denotes the reduction of longitudinal confinement of light due to external cavity. This is accomplished by the introduction of high-Q passive resonator or long delay line in the external cavity. (14) represents the contribution of the detuned loading effect, which arises from the coupling of gain and refractive index through carrier density in semiconductor laser [44]. Interestingly, a high α_{H} is desirable in order to maximize the linewidth reduction from the external cavity. Since α_{H} appears on both the numerator and denominator of (11), it is informative

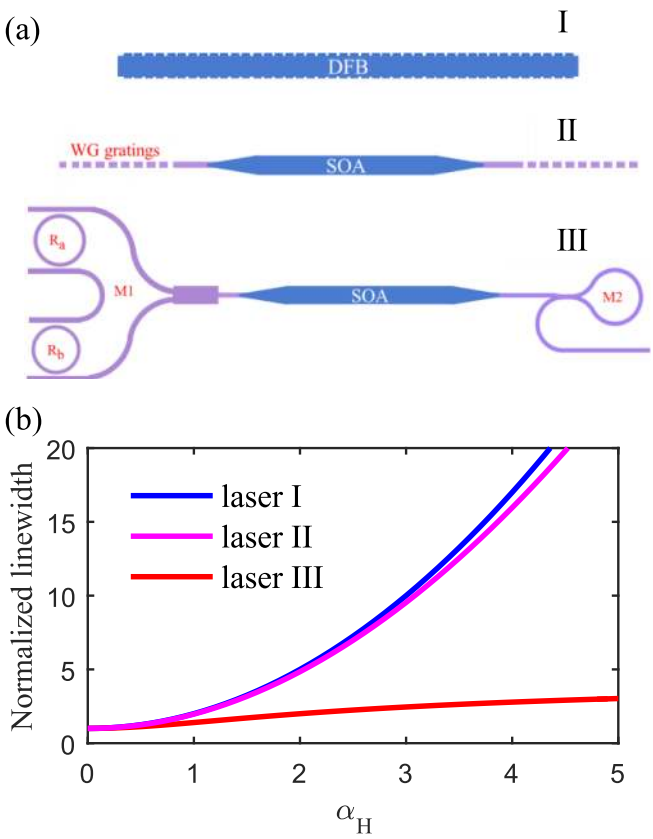

Fig. 5. (a) Existing laser designs to achieve narrow linewidth operation in semiconductor lasers. I: DFB laser. II: DBR laser with passive waveguide grating. III: external cavity laser with two high-Q ring resonators in one of the loop mirrors. SOA: semiconductor optical amplifier. (b) Dependence of laser linewidth on linewidth enhancement factor in each laser design. The calculated linewidth is normalized with respect to 0 α_{H} scenario. The detailed calculation procedure and parameters can be found in Appendix B.

to look into the overall effect of α_{H} on the laser linewidth. Fig. 5(a) illustrates three designs to achieve narrow linewidth operation in a semiconductor laser. The first design is that of a distributed feedback (DFB) laser. In a heterogeneous integration platform, laser linewidth of 18 kHz has been achieved [43]. The second design is that of a distributed Bragg reflector (DBR) laser. By having long DBR mirrors in the external cavity in low loss silicon or silicon nitride platforms, the longitudinal confinement factor can be significantly reduced to have a large A factor. The third design involves forming high-Q resonators in a waveguide loop mirror in the external cavity. Not only does the high Q factor in the ring resonator enhance the A factor, the sharp filtering response of these resonators results in a large B factor. Using realistic external cavity design parameters, the normalized laser linewidth as a function α_{H} is shown in 5(b) for each of the laser design in 5(a).

In all three cases, a smaller α_{H} corresponds to narrower linewidth. In a DFB laser the dependence of linewidth on α_{H} follows strictly the $1+\alpha_{\mathrm{H}}^2$ relationship in (2). Assuming the same α_{H} for QW and QD lasers as used in the feedback sensitivity analysis, the linewidth in QD DFB lasers should be 13% of that in a monolithic QW DFB laser, which typically exhibits linewidth of a few MHz. In comparison, intrinsic

TABLE I
SIMULATION PARAMETERS USED FOR FIG. 4

Parameter	QD laser in this work
Differential quantum efficiency	0.35
Photon lifetime (ps)	2.04
Differential carrier lifetime (ns)	0.157
Gain compression factor (cm^3)	5×10^{-16}
Differential gain wrt. carrier density (cm^2)	3.18×10^{-15}
Differential gain wrt. photon density (cm^2)	3.94×10^{-13}

linewidth as low as 80 kHz has been reported in QD DFB lasers [45], [46]. For external cavity DBR lasers, the majority of F is from A due to the relatively flat mirror response at peak mirror reflection. Consequently, F is a weak function of α_{H}, making the overall dependence on α_{H} similar to that in the DFB laser. For an external cavity laser with high-Q resonators as part of the waveguide mirror, the B factor dominates F because of the sharp filter responses of the resonators. Only 50% reduction in linewidth can be achieved by replacing the QW active region with the QD counterpart. However, the lowest linewidth in diode lasers by far is reported for lasers integrated with high-Q resonator. Further reduction in linewidth with QD active region is still invaluable.

VI. CONCLUSION

We have shown experimentally and theoretically the critical role dot uniformity plays in achieving ultra small α_{H} in QD lasers. In addition, the introduction of modulation *p* doping in the QD active region further reduces α_{H}. By adjusting the amount of *p*-doping in the QD active region, one can even engineer α_{H} to suit the target application. With small α_{H} and high damping frequency, QD lasers have been shown to exhibit much higher feedback tolerance compared to QW lasers. The ultra-stable operation of QD lasers make it possible to construction laser systems without co-packaged optical isolators. Last but not least, the small α_{H} in QD lasers has been shown to significantly reduce laser linewidth compared to QW lasers in all existing narrow linewidth laser designs.

APPENDIX A
QUANTUM DOT LASER PARAMETER EXTRACTION

After measuring the ASE spectra of the QD lasers, the net modal gain as a function of current is measured using the mode-sum method [23]. Laser transparency is then measured at the gain-peak wavelength using the Andrekson method [47], which enables the extraction of total optical loss (threshold gain) of the laser [17]. Since the calculated material gain is obtained at different carrier density, comparing the measured material gain with the simulation results allows the extraction of carrier recombination coefficients. The key parameters in the laser modulation response including differential gain, photon life time, and differential carrier life time can then be calculated from the extracted quantities. The laser relaxation oscillation is modeled using a compact rate equation model implemented similarly to the one detailed in [48]. The parameters used for Fig. 4 are listed in Table I.

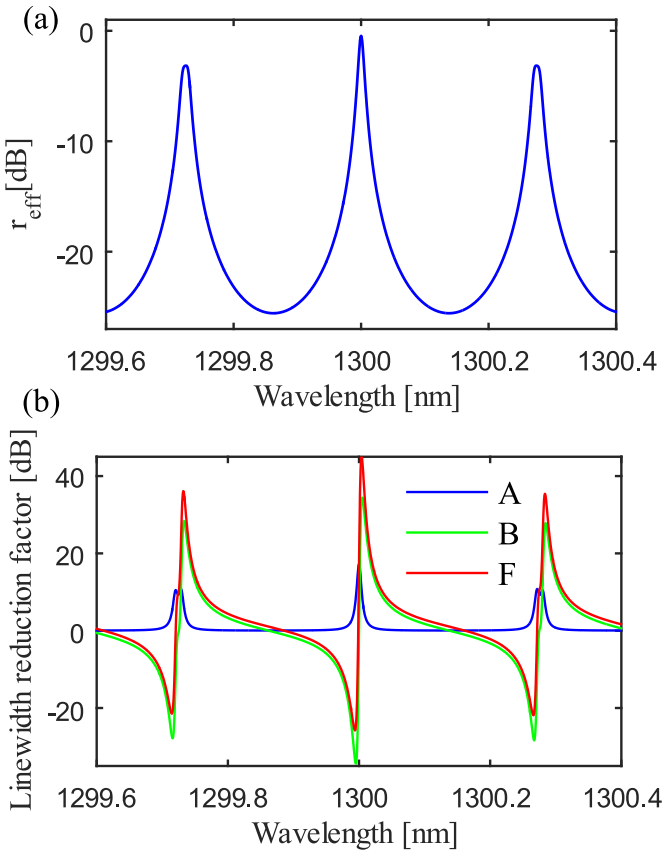

Fig. 6. (a) Effective mirror response of the external cavity laser in Fig. 5(a) III. In this simulation, $K = 0.1$, $\alpha = 3\ \mathrm{m}^{-1}$, $R_{\mathrm{a}} = 300\ \mu$m and $R_{\mathrm{b}} = 310\ \mu$m. (b) The linewidth reduction factor for the same laser design calculated based on (12)–(14).

APPENDIX B
LINEWIDTH REDUCTION FACTOR CALCULATION

This section will give an example of how linewidth reduction factor is calculated for an external cavity laser. The vernier ring external cavity laser design in Fig. 5(a) will be analyzed here. In this laser, both waveguide loop mirrors are broadband and offer little wavelength selectivity. Therefore, the mirror response is described by the transmission over the two high-Q ring resonators:

$$r_1 = T_{\mathrm{ra}} T_{\mathrm{rb}} = \frac{\kappa_{\mathrm{a1}}^* \kappa_{\mathrm{a2}}^* \eta_{\mathrm{a}}^{0.5}}{1 - \eta_{\mathrm{a}} t_{\mathrm{a1}}^* t_{\mathrm{a2}}^*} \frac{\kappa_{\mathrm{b1}}^* \kappa_{\mathrm{b2}}^* \eta_{\mathrm{b}}^{0.5}}{1 - \eta_{\mathrm{b}} t_{\mathrm{b1}}^* t_{\mathrm{b2}}^*} \tag{15}$$

$$\eta_{\mathrm{a}} = e^{-(j\beta+\alpha)2\pi R_{\mathrm{a}}} \tag{16}$$

$$\eta_{\mathrm{b}} = e^{-(j\beta+\alpha)2\pi R_{\mathrm{b}}} \tag{17}$$

where κ_{in} and t_{in} are the cross-coupled and through-coupled field coefficients for ring i and port n, η_{i} is the round-trip phase and loss accumulation in ring i, R_i is the radius for ring i, β is the wave number, α is the field attenuation coefficient in the waveguide and j is the imaginary unit. The computed effective mirror response and the corresponding linewidth reduction factor are shown in Fig. 6. As expected from the physical

interpretation of A and B, the maxima of A occur at the resonance wavelength of the resonators while the maxima of B are detuned to the red side of each resonance peak. Since F is dominated by B, the maxima of F are detuned from the resonance peaks of the ring resonators as well.

ACKNOWLEDGMENT

The authors are thankful to Frédéric Grillot for meaningful discussions and M. J. Kennedy for device fabrication. Stella Meng and Yoyo Meng offered a great deal of moral support throughout the duration of this project.

REFERENCES

[1] M. W. Fleming and A. Mooradian, "Fundamental line broadening of single-mode (GaAl)As diode lasers," *Appl. Phys. Lett.*, vol. 38, no. 7, pp. 511–513, 1981.

[2] C. Henry, "Theory of the linewidth of semiconductor lasers," *IEEE J. Quantum Electron.*, vol. QE-18, no. 2, pp. 259–264, Feb. 1982.

[3] K. Vahala and A. Yariv, "Semiclassical theory of noise in semiconductor lasers—Part II," *IEEE J. Quantum Electron.*, vol. QE-19, no. 6, pp. 1102–1109, Jun. 1983.

[4] R. Tkach and A. Chraplyvy, "Regimes of feedback effects in 1.5 μm distributed feedback lasers," *J. Lightw. Technol.*, vol. LT-4, no. 11, pp. 1655–1661, Nov. 1986.

[5] J. Helms and K. Petermann, "A simple analytic expression for the stable operation range of laser diodes with optical feedback," *IEEE J. Quantum Electron.*, vol. 26, no. 5, pp. 833–836, May 1990.

[6] J. Helms and K. Petermann, "Microwave modulation of laser diodes with optical feedback," *J. Lightw. Technol.*, vol. 9, no. 4, pp. 468–476, Apr. 1991.

[7] R. Lang and K. Kobayashi, "External optical feedback effects on semiconductor injection laser properties," *IEEE J. Quantum Electron.*, vol. QE-16, no. 3, pp. 347–355, Mar. 1980.

[8] W. Rideout *et al.*, "Measurement of the carrier dependence of differential gain, refractive index, and linewidth enhancement factor in strained-layer quantum well lasers," *Appl. Phys. Lett.*, vol. 56, no. 8, pp. 706–708, 1990.

[9] U. Schwarz *et al.*, "Optical gain, carrier-induced phase shift, and linewidth enhancement factor in InGaN quantum well lasers," *Appl. Phys. Lett.*, vol. 83, no. 20, pp. 4095–4097, 2003.

[10] M. Osinski and J. Buus, "Linewidth broadening factor in semiconductor lasers—An overview," *IEEE J. Quantum Electron.*, vol. QE-23, no. 1, pp. 9–29, Jan. 1987.

[11] I. Coddington, N. Newbury, and W. Swann, "Dual-comb spectroscopy," *Optica*, vol. 3, no. 4, pp. 414–426, 2016.

[12] Z. Newman *et al.*, "Photonic integration of an optical atomic clock," 2018, *arXiv:1811.00616*.

[13] Y. Arakawa, K. Vahala, A. Yariv, and K. Lau, "Reduction of the spectral linewidth of semiconductor lasers with quantum wire effects-spectral properties of GaAlAs double heterostructure lasers in high magnetic fields," *Appl. Phys. Lett.*, vol. 48, no. 6, pp. 384–386, 1986.

[14] Y. Arakawa, K. Vahala, and A. Yariv, "Quantum noise and dynamics in quantum well and quantum wire lasers," *Appl. Phys. Lett.*, vol. 45, no. 9, pp. 950–952, 1984.

[15] D. Bimberg *et al.*, "InGaAs–GaAs quantum-dot lasers," *IEEE J. Sel. Topics Quantum Electron.*, vol. 3, no. 2, pp. 196–205, Apr. 1997.

[16] W. W. Chow and F. Jahnke, "On the physics of semiconductor quantum dots for applications in lasers and quantum optics," *Progress Quantum Electron.*, vol. 37, no. 3, pp. 109–184, 2013.

[17] D. Jung *et al.*, "Impact of threading dislocation density on the lifetime of InAs quantum dot lasers on Si," *Appl. Phys. Lett.*, vol. 112, no. 15, 2018, Art. no. 153507.

[18] O. Shchekin and D. Deppe, "1.3 μm InAs quantum dot laser with $T_o =$ 161 K from 0 to 80 °C," *Appl. Phys. Lett.*, vol. 80, no. 18, pp. 3277–3279, 2002.

[19] O. Shchekin and D. Deppe, "The role of p-type doping and the density of states on the modulation response of quantum dot lasers," *Appl. Phys. Lett.*, vol. 80, no. 15, pp. 2758–2760, 2002.

[20] Z. Zhang *et al.*, "Effects of modulation p doping in InAs quantum dot lasers on silicon," *Appl. Phys. Lett.*, vol. 113, no. 6, 2018, Art. no. 061105.

[21] D. Jung *et al.*, "Highly reliable low-threshold InAs quantum dot lasers on on-axis (001) Si with 87% injection efficiency," *ACS Photon.*, vol. 5, no. 3, pp. 1094–1100, 2017.

[22] "Next**nano**^{3}." [Online]. Available: http://www.nextnano.com/nextnano3/. Accessed: Apr. 18, 2018.

[23] D. T. Cassidy, "Technique for measurement of the gain spectra of semiconductor diode lasers," *J. Appl. Phys.*, vol. 56, no. 11, pp. 3096–3099, 1984.

[24] W. W. Chow and S. W. Koch, "Theory of semiconductor quantum-dot laser dynamics," *IEEE J. Quantum Electron.*, vol. 41, no. 4, pp. 495–505, Apr. 2005.

[25] H. Schneider, W. Chow, and S. W. Koch, "Anomalous carrier-induced dispersion in quantum-dot active media," *Phys. Rev. B*, vol. 66, no. 4, 2002, Art. no. 041310.

[26] A. Ukhanov, A. Stintz, P. Eliseev, and K. Malloy, "Comparison of the carrier induced refractive index, gain, and linewidth enhancement factor in quantum dot and quantum well lasers," *Appl. Phys. Lett.*, vol. 84, no. 7, pp. 1058–1060, 2004.

[27] K. J. Vahala and C. Zah, "Effect of doping on the optical gain and the spontaneous noise enhancement factor in quantum well amplifiers and lasers studied by simple analytical expressions," *Appl. Phys. Lett.*, vol. 52, no. 23, pp. 1945–1947, 1988.

[28] J. Duan *et al.*, "Semiconductor quantum dot lasers epitaxially grown on silicon with low linewidth enhancement factor," *Appl. Phys. Lett.*, vol. 112, no. 25, 2018, Art. no. 251111.

[29] "CW tunalbe laser, butterfly package." [Online]. Avaliable: https://www.finisar.com/communication-components/s7500. Accessed: Dec. 13, 2018.

[30] "External cavity single-frequency laser, butterfly package." [Online]. Available: https://www.thorlabs.com/newgrouppage9.cfm?objectgroup_id=4934. Accessed: Dec. 13, 2018.

[31] L. A. Coldren, S. W. Corzine, and M. L. Mashanovitch, *Diode Lasers and Photonic Integrated Circuits*. Hoboken, NJ, USA: Wiley, 2012, vol. 218.

[32] J. Mork, B. Tromborg, and J. Mark, "Chaos in semiconductor lasers with optical feedback: Theory and experiment," *IEEE J. Quantum Electron.*, vol. 28, no. 1, pp. 93–108, Jan. 1992.

[33] J. O. Binder and G. D. Cormack, "Mode selection and stability of a semiconductor laser with weak optical feedback," *IEEE J. Quantum Electron.*, vol. 25, no. 11, pp. 2255–2259, Nov. 1989.

[34] C. Hantschmann *et al.*, "Understanding the bandwidth limitations in monolithic 1.3 μm InAs/GaAs quantum dot lasers on silicon," *J. Lightw. Technol.*, vol. 37, no. 3, pp. 949–955, Feb. 2019.

[35] F. Grillot, B. Dagens, J.-G. Provost, H. Su, and L. F. Lester, "Gain compression and above-threshold linewidth enhancement factor in 1.3 μm InAs-GaAs quantum dot lasers," *IEEE J. Quantum Electron.*, vol. 44, no. 10, pp. 946–951, Oct. 2008.

[36] D. Inoue *et al.*, "Directly modulated 1.3 μm quantum dot lasers epitaxially grown on silicon," *Opt. Express*, vol. 26, no. 6, pp. 7022–7033, 2018.

[37] M. Ishida *et al.*, "Effect of carrier transport on modulation bandwidth of 1.3-μ m InAs/GaAs self-assembled quantum-dot lasers," in *Proc. 22nd IEEE Int. Semicond. Laser Conf*, 2010, pp. 174–175.

[38] P. J. Thijs, L. F. Tiemeijer, P. Kuindersma, J. Binsma, and T. Van Dongen, "High-performance 1.5 μm wavelength InGaAs–InGaAsP strained quantum well lasers and amplifiers," *IEEE J. Quantum Electron.*, vol. 27, no. 6, pp. 1426–1439, Jun. 1991.

[39] Y. Hirayama, M. Morinaga, N. Suzuki, and M. Nakamura, "Extremely reduced nonlinear k-factor in high-speed strained layer multiquantum well DFB lasers," *Electron. Lett.*, vol. 27, no. 10, pp. 875–876, 1991.

[40] P. Blood, "Quantum efficiency of quantum dot lasers," *IEEE J. Sel. Topics Quantum Electron.*, vol. 23, no. 6, Nov./Dec. 2017, Art. no. 1900608.

[41] H. Huang *et al.*, "Analysis of the optical feedback dynamics in InAs/GaAs quantum dot lasers directly grown on silicon," *JOSA B*, vol. 35, no. 11, pp. 2780–2787, 2018.

[42] R. Kazarinov and C. Henry, "The relation of line narrowing and chirp reduction resulting from the coupling of a semiconductor laser to passive resonator," *IEEE J. Quantum Electron.*, vol. QE-23, no. 9, pp. 1401–1409, Sep. 1987.

[43] C. T. Santis, S. T. Steger, Y. Vilenchik, A. Vasilyev, and A. Yariv, "High-coherence semiconductor lasers based on integral high-q resonators in hybrid Si/III-V platforms," *Proc. Nat. Acad. Sci.*, vol. 111, no. 8, pp. 2879–2884, 2014.

[44] T. Komljenovic *et al.*, "Widely tunable narrow-linewidth monolithically integrated external-cavity semiconductor lasers," *IEEE J. Sel. Topics Quantum Electron.*, vol. 21, no. 6, Nov./Dec. 2015, Art. no. 1501909.

[45] J. Duan *et al.*, "Narrow spectral linewidth in InAs/InP quantum dot distributed feedback lasers," *Appl. Phys. Lett.*, vol. 112, no. 12, 2018, Art. no. 121102.
[46] A. Becker *et al.*, "Widely tunable narrow-linewidth 1.5 μm light source based on a monolithically integrated quantum dot laser array," *Appl. Phys. Lett.*, vol. 110, no. 18, 2017, Art. no. 181103.
[47] P. Andrekson *et al.*, "Novel technique for determining internal loss of individual semiconductor lasers," *Electron. Lett.*, vol. 28, no. 2, pp. 171–172, 1992.
[48] Z. Zhang *et al.*, "Compact modeling for silicon photonic heterogeneously integrated circuits," *J. Lightw. Technol.*, vol. 35, no. 14, pp. 2973–2980, Jul. 2017.

Zeyu Zhang (S'17) received the B.S. degree in electrical engineering from Clemson University, Clemson, SC, USA, in 2015. He is currently working toward the Ph.D. degree with the University of California Santa Barbara, Santa Barbara, CA, USA.

His research interests include characterization and modeling of quantum dot laser epitaxially grown on silicon as well as passive–active integration of photonic devices with quantum dot active region on monolithic III–V on silicon platforms.

Daehwan Jung (M'16) received the Ph.D. degree in electrical engineering from Yale University, New Haven, CT, USA, in 2016. He is currently with the Korea Institute of Science and Technology, Center for Opto-Electronic Materials and Devices, Seoul, South Korea.

His primary research interest is to study novel III–V materials growth for high-performance optoelectronic and photonic devices. His current research project is to develop highly reliable, high-performance quantum dot lasers epitaxially grown on silicon for communication applications.

Justin Norman (S'14) received B.S. degree in chemical engineering and physics from the University of Arkansas at Fayetteville, Fayetteville, AR, USA, in 2013, and the Ph.D. degree in materials from the University of California Santa Barbara, Santa Barbara, CA, USA, in 2018. He is the recipient of both the National Science Foundation Graduate Research Fellowship and the Frenkel Foundation Fellowship. He is currently with the University of California Santa Barbara, as a Postdoctoral Researcher.

His research interests are in the growth of InAs quantum dots via molecular beam epitaxy for applications in photonics and quantum electrodynamics. He also works on the heteroepitaxy of III–V materials on Si for photonic integration.

Weng W. Chow (F'09) received the Ph.D. degree in physics from the University of Arizona, Tucson, AZ, USA, on research involving fluctuation phenomena in quantum optics. He is currently a Technical Staff Member with Sandia National Laboratories, Albuquerque, NM, USA, where his primary research involves applying microscopic theory to semiconductor laser development. Some of this work is described in two texts—*Semiconductor Laser Physics* and *Semiconductor Laser Fundamentals: Physics of the Gain Materials*.

He is also the Honorary Professor of physics with Cardiff University, Cardiff, U.K., and a Fellow with the Institute for Quantum Science and Engineering at Texas A&M University. He is a Fellow of the Optical Society of America. He is the recipient of the Department of Energy, Basic Energy Science/Material Science Award, the J. J. Thompson Premium, the LEOS Distinguished Lecturer Award, the Alexander von Humboldt Senior Scientist Award, and the IEEE Photonics Society Quantum Electronics Award.

John E. Bowers (F'93) received the M.S. and Ph.D. degrees from Stanford University, Stanford, CA, USA. He is currently the Fred Kavli Chair in Nanotechnology, the Director of the Institute for Energy Efficiency, and a Professor with the Department of Electrical and Computer Engineering and Materials Department, University of California Santa Barbara (UCSB), Santa Barbara, CA, USA. He is a Co-Founder of Aurrion, Aerius Photonics, and Calient Networks. He was with AT&T Bell Laboratories and Honeywell before joining UCSB. His research is primarily in optoelectronics and photonic integrated circuits. He has authored/coauthored ten book chapters, 600 journal papers, 900 conference papers, and has received 54 patents. He is a member of the National Academy of Engineering and a Fellow of the Optical Society of America (OSA) and the American Physical Society. He is a recipient of the OSA/IEEE Tyndall Award, the OSA Holonyak Prize, the IEEE LEOS William Streifer Award, and the South Coast Business and Technology Entrepreneur of the Year Award. He and his coworkers received the EE Times Annual Creativity in Electronics (ACE) Award for Most Promising Technology for the heterogeneous silicon laser in 2007.